ADVANCED MATERIALS
www.advmat.de

A Stimulus-Responsive Zinc–Iodine Battery with Smart Overcharge Self-Protection Function

Faxing Wang, Jochi Tseng, Zaichun Liu, Panpan Zhang, Gang Wang, Guangbo Chen, Weixing Wu, Minghao Yu, Yuping Wu, and Xinliang Feng**

Zinc–iodine aqueous batteries (ZIABs) are highly attractive for grid-scale energy storage due to their high theoretical capacities, environmental friendliness, and intrinsic non-flammability. However, because of the close redox potential of Zn stripping/platting and hydrogen evolution, slight overcharge of ZIABs would induce drastic side reactions, serious safety concerns, and battery failure. A novel type of stimulus-responsive zinc–iodine aqueous battery (SR-ZIAB) with fast overcharge self-protection ability is demonstrated by employing a smart pH-responsive electrolyte. Operando spectroelectrochemical characterizations reveal that the battery failure mechanism of ZIABs during overcharge arises from the increase of electrolyte pH induced by hydrogen evolution as well as the consequent irreversible formation of insulating ZnO at anode and soluble $Zn(IO_3)_2$ at cathode. Under overcharge conditions, the designed SR-ZIABs can be rapidly switched off with capacity degrading to 6% of the initial capacity, thereby avoiding continuous battery damage. Importantly, SR-ZIABs can be switched on with nearly 100% of capacity recovery by re-adjusting the electrolyte pH. This work will inspire the development of aqueous Zn batteries with smart self-protection ability in the overcharge state.

Stimulus-responsive materials and devices are attracting intensive attention because of the ever-increasing demand for intelligent devices.[1–6] In particular, integrating stimulus-responsive functions into rechargeable batteries shows great potential to revolutionize electrochemical energy storage systems for future smart devices.[7–24] Currently, the three most eye-catching stimulus-responsive batteries are temperature-responsive Li-ion batteries,[11,14,16,20] photo-responsive Li-ion batteries,[7,17,18] and self-healing Li-ion batteries.[8,13,15,19] Despite the availability of aforementioned stimulus-responsive batteries, the developed stimulus responses for rechargeable batteries are still sparse owing to the complexity and compatibility of battery architectures.[24] Moreover, the reported stimulus-responsive functions are mainly integrated into Li-ion batteries.[8,13–20] However, the limited Li resources and high flammability of Li-ion batteries severely impede their commercial applications for stationary energy storage systems. Therefore, it is highly desired to explore new stimulus-responsive systems beyond Li-ion batteries.

As prospective alternatives for Li-ion batteries, rechargeable zinc-iodine aqueous batteries (ZIABs) are emerging for large-scale energy storage systems because of high theoretical capacities and energy densities (around 169 mAh g^{-1} and 220 Wh kg^{-1} based on the total mass of active cathode and anode materials), abundant raw materials, environmental friendliness, non-flammable aqueous electrolytes, and simplified battery packaging technology in air.[25–34] However, ZIABs suffer from the serious overcharge problem due to the close redox potentials of Zn stripping/platting and hydrogen (H_2) evolution.[35–38] For example, a recent pressure sensor analysis of Zn anode in a slightly acidic electrolyte (pH = 4.57) manifested the side reaction rate of H_2 evolution up to 3×10^{-7} moles per cycle.[38] Generally, even slight overcharge of ZIABs promotes the decomposition of aqueous electrolyte, leading to the undesired H_2 generation at Zn anode. The gas generation in ZIABs at overcharge state would cause internal pressure rise and swelling/cracking of the battery package,[39] thus limiting the market acceptance of ZIABs for practical applications. Currently, the most general way to release the internal gas pressure of commercialized aqueous batteries is to design safety vents on battery packages.[39] Nevertheless, safety vents cannot alleviate

F. Wang, Dr. P. Zhang, Dr. G. Wang, G. Chen, Dr. M. Yu, Prof. X. Feng
Center for Advancing Electronics Dresden (cfaed) & Department of Chemistry and Food Chemistry
Technische Universität Dresden
Mommsenstrasse 4, Dresden 01069, Germany
E-mail: minghao.yu@tu-dresden.de; xinliang.feng@tu-dresden.de
Dr. J. Tseng
Deutsches Elektronen-Synchrotron (DESY)
Hamburg 22607, Germany
Z. Liu, Prof. Y. Wu
State Key Laboratory of Materials-oriented Chemical Engineering
School of Energy
Science and Engineering
Nanjing Tech University
Nanjing 211816, China
W. Wu
School of Chemistry
Sun Yat-sen University
Guangzhou 510275, China

The ORCID identification number(s) for the author(s) of this article can be found under https://doi.org/10.1002/adma.202000287.

DOI: 10.1002/adma.202000287

or suppress the irreversible gas evolution at overcharge state, which will lead to continuous battery damage. Besides, the complicated electrode side reactions in ZIABs induced by overcharge remain elusive. Accordingly, in-depth understanding of the battery failure mechanism for ZIABs during overcharge processes and finding an efficient approach to immediately switch off the overcharged ZIABs are of particular importance for accelerating the practical application of ZIABs.

Herein, we demonstrate a novel kind of stimulus-responsive zinc-iodine aqueous batteries (SR-ZIABs) with smart overcharge self-protection ability, which can rapidly switch off the redox reactions and avoid the gas generation once SR-ZIABs are overcharged. Conventional ZIABs under overcharge are revealed to encounter an apparent pH increase from 4.3 to 5.9, which results in the fast performance decay. Operando spectroelectrochemical investigations and theoretical simulations disclose that the battery failure of ZIABs under overcharge is associated with the irreversible formation of insulating ZnO at the anode and soluble $Zn(IO_3)_2$ at the cathode. The SR-ZIABs are assembled employing a smart pH-responsive electrolyte based on poly(2-vinylpyridine) (P2VP). The pH increase in the overcharged SR-ZIABs induces the fast transition of P2VP from hydrophilic soluble state to hydrophobic gel state in less than 30 s due to the de-protonation of quaternary pyridinic groups in electrolyte, which lead to the internal resistance increase of the overcharged SR-ZIABs by four orders of magnitude (**Figure 1**). Thereby, SR-ZIABs under overcharge conditions can be rapidly switched off with capacity degradation to 6% of the initial capacity, avoiding the continuous battery damage. Importantly, the switched-off SR-ZIABs can recover to the normal operation state with 100% capacity recovery via re-adjusting the electrolyte pH to the initial state.

ZIABs studied in this work are composed of iodine/N-doped-carbon (I_2/N-C) cathode (Figures S1–S4, Supporting Information), glass fiber separator, Zn anode, and 1 M $ZnSO_4$ aqueous electrolyte. To identify the maximum normal operating voltage, ZIABs are slowly charged/discharged at 0.3 A g^{-1} with various cut-off voltages (Figure S5, Supporting Information). The plots of Coulombic efficiencies of ZIABs as a function of cut-off voltages (**Figure 2**a) show three distinct regions. When the cut-off voltage is below 1.6 V, the Coulombic efficiency is close to 100% (e.g., 99.5% at 1.6 V), indicating the normal operation of the battery. Once the voltage exceeds 1.6 V, the Coulombic efficiency drops rapidly (e.g., 92% at 1.65 V and 85% at 1.85 V), implying that irreversible reactions take place in ZIABs. When the cut-off voltage reaches 1.95 V, the drastic irreversible reactions are identified by the low Coulombic efficiency of only 56%. Thereby, the maximum normal charge cut-off voltage for ZIABs is recognized to be 1.6 V. Electrolyte pH also serves as an effective indicator for the suitable operating voltage of ZIABs. Figure 2b displays the electrolyte pH of ZIABs at various charge/discharge states, which can be monitored by a pH meter. As revealed, the electrolyte pH of ZIABs experiences negligible change from ≈4.3 to ≈4.5 in the voltage window of 0.6–1.6 V. Notably, when the charge voltage is over 1.6 V, the electrolyte pH tends to increase rapidly. Once the ZIABs are continually charged to 1.95 V, the electrolyte pH increases to ≈5.9. The apparent increase of electrolyte pH is ascribed to the side reaction of H_2 evolution at the Zn anode (Figure S6, Supporting Information).[38] When the voltage of ZIABs is higher than 1.9 V, although H_2 evolution continues to produce OH^- on the anode surface, oxygen evolution also occurs on the cathode surface and produce H^+. Thus, the electrolyte pH appears to be stable at a voltage of around 1.9 V.

The electrochemical behavior of ZIABs under normal operation (0.6–1.6 V) and overcharge operation (0.6–1.95 V) are further compared to clarify the influence of overcharge on the performance degradation of ZIBs. When ZIABs are operated in the voltage of 0.6–1.6 V (Figure 2c; Figure S7, Supporting Information), one pair of cathodic/anodic peaks at 1.15/1.3 V can be observed in the cyclic voltammetry (CV) curve at 2 mV s^{-1}, corresponding to the reversible conversion reaction between ZnI_2 and I_2.[26,27,40] In the subsequent 10 cycles, CV curves remain almost unchanged, which implies the high reversibility of ZIABs. Galvanostatic charge/discharge measurements with current densities ranging from 0.14 to 5.7 A g^{-1} are also conducted

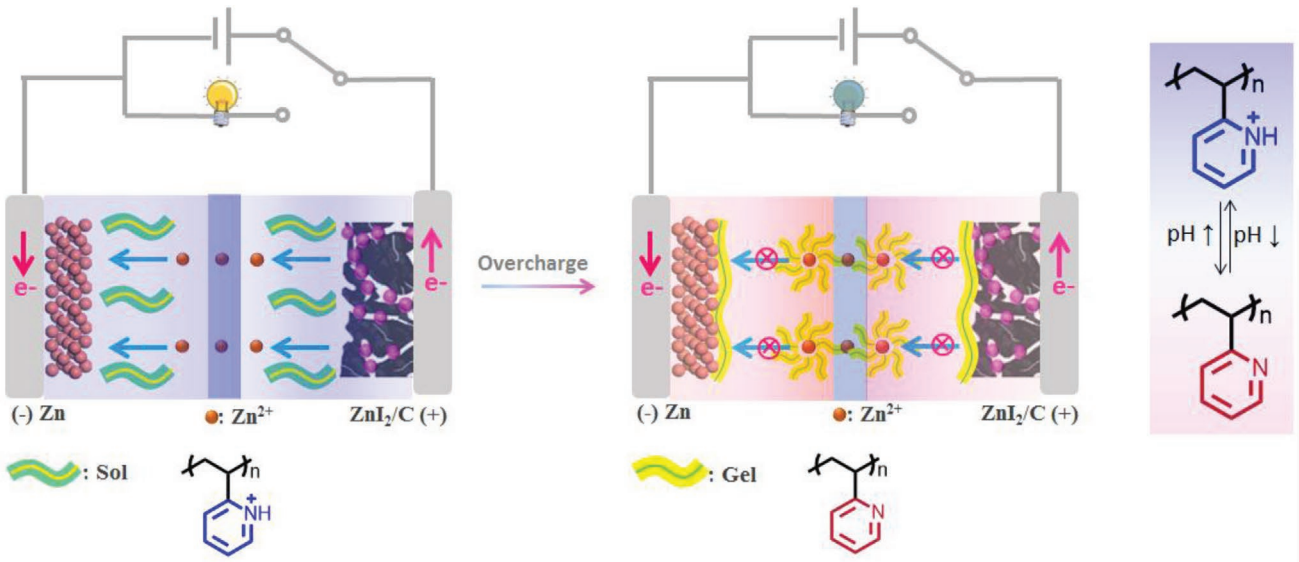

Figure 1. Illustration of the self-protection function of SR-ZIABs.

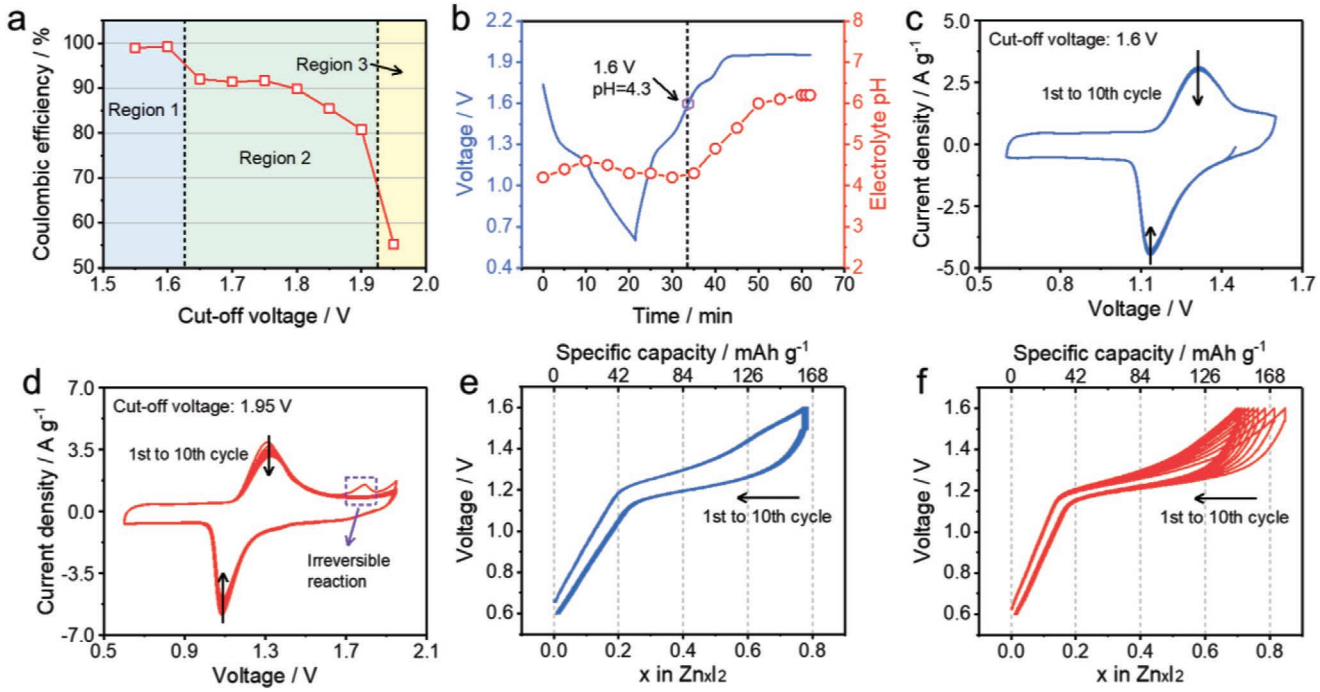

Figure 2. The electrochemical behavior of ZIABs. a) The Coulombic efficiencies of ZIABs at 0.3 A g^{-1} with different cut-off voltages. b) The electrolyte pH variation during the discharge/charge processes of ZIABs. The CV curves of ZIABs at 2 mV s^{-1} with the voltage window of c) 0.6–1.6 V and d) 0.6–1.95 V. Galvanostatic charge/discharge curves of ZIABs e) before and f) after overcharge to 1.95 V.

for ZIABs in the voltage of 0.6–1.6 V. The maximum specific capacity of ZIABs based on the mass of I_2/N-C cathode reaches 193 mA h g^{-1} at 0.14 A g^{-1} (Figure S8a, Supporting Information). When the current density increases to 5.7 A g^{-1}, ZIABs still deliver a reversible capacity of 128 mAh g^{-1} (Figure S8a, Supporting Information). The maximum energy density of ZIABs reaches 220 Wh kg^{-1} based on the mass of the active I_2/N-C cathode material (Figure S8b, Supporting Information). After 250 cycles in a voltage window of 0.6–1.6 V, ZIABs are able to maintain 85% of its initial capacity (Figure S9, Supporting Information). In contrast, when ZIABs are operated with an overcharge voltage window (0.6–1.95 V), a new cathodic peak emerges at around 1.8 V in the CV curves, which is irreversible without corresponding anodic peak (Figure 2d). Meanwhile, the current density of redox peaks for ZIABs operated in the overcharge voltage window gradually decreases in the following cycles (Figures 2d; Figure S10a, Supporting Information). Furthermore, the influence of overcharge on the cycling stability of ZIABs is assessed. Under normal voltage window of 0.6–1.6 V, ZIABs show a slow capacity decay rate of only ≈0.03% per cycle during the initial 10 cycles (Figure 2e). By contrast, after the overcharge to 1.95 V, ZIABs exhibit severe capacity decay from 177 mAh g^{-1} at the first cycle to 145 mAh g^{-1} at the 10th cycle, with a decay rate of ≈1.8% per cycle (Figure 2f). The capacity decay rate of the overcharged ZIABs increases by 60 times compared with that of the normal operated ZIABs. More seriously, the soft package of ZIABs swells a lot after ZIABs are overcharged to 1.95 V for 20 min (Figure S10b, Supporting Information).

To figure out the battery failure mechanism of the overcharged ZIABs, operando synchrotron X-ray diffraction (Figure S11, Supporting Information) and ultraviolet–visible (UV–vis) spectroscopy (Figure S12, Supporting Information) analyses were performed during the charge process of ZIABs. **Figure 3**a displays the operando synchrotron X-ray diffraction patterns of the Zn anode during the charge process of ZIABs. Along with the charge of ZIABs to 1.6 V, the intensities of two peaks at 6.15 and 9.67 $Å^{-1}$ gradually increase, which can be ascribed to the continuous plating of Zn at anode. When ZIABs is overcharged to 1.85 V, there are three new peaks located at 10.44, 13.74, and 13.78 $Å^{-1}$ (Figure 3a; Figure S13, Supporting Information), which are indexed to the {002} {202} and {004} crystal facets of ZnO, respectively.[41] It was previously reported that, in Zn-ion batteries using $ZnSO_4$ electrolyte, precipitated zinc hydroxide sulfate ($Zn_4(OH)_6SO_4 \cdot 5H_2O$) was observed during the discharge process, and then dissolved into the electrolyte during the charge process.[42,43] For the charge process of ZIABs, operando synchrotron X-ray diffraction analysis reveals a probable equilibrium reaction (Figure S13b, Supporting Information) between the dissolved $Zn_4(OH)_6SO_4 \cdot 5H_2O$ and ZnO at Zn anode surface (Equation (1)). At the overcharge state, the continuous H^+ consumption breaks the equilibrium reaction and promotes the transformation of the intermediate $Zn_4(OH)_6SO_4 \cdot 5H_2O$ to ZnO at the Zn anode. The irreversible formation of ZnO under the overcharge condition would reduce the electrochemical activity of Zn anode because of the poor conductivity of ZnO.

$$Zn_4(OH)_6SO_4 \cdot 5H_2O \leftrightarrow 4ZnO + 2H^+ + SO_4^{2-} + 7H_2O \quad (1)$$

The operando UV–vis spectroscopy analysis on the electrolyte also offers important insight into the interaction between I_2/N-C cathode and electrolyte. During the charge process of

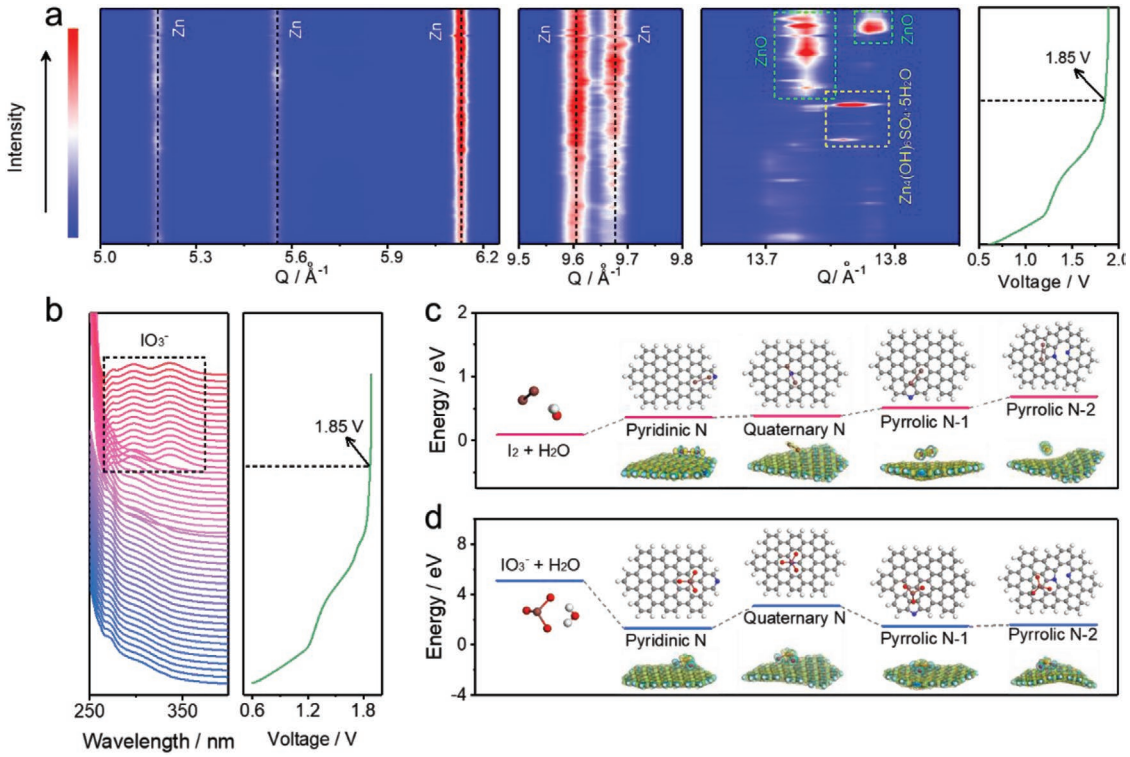

Figure 3. The mechanism studies of electrochemical behavior for ZIABs at overcharge state. a) The operando synchrotron X-ray diffraction of the Zn anode during the charge process of ZIABs. b) The operando UV–vis spectroscopy of the electrolyte during the charge process of ZIABs. c) I_2 and d) IO_3^- solvation energy as well as their interaction energy with N-doped carbon substrate calculated by DFT. Four typical N-doped carbon structures are simulated, including one quaternary, one pyridinic, and two pyrrolic N structures. Insets show the stabilized configurations and corresponding charge density differences.

ZIABs in the normal voltage (0.6–1.6 V), the discharge product (ZnI_2) is oxidized to I_2.[26,27,40] When the charging voltage of ZIABs reaches 1.85 V, a new UV–vis absorption peak at 340 nm appears (Figure 3b), which is attributed to the iodate (IO_3^-) (Figure S14, Supporting Information). The detected IO_3^- intermediate arises from the excessive oxidation of I_2 during overcharge process of ZIABs according to Equation (2). This irreversible reaction is in consistent with the observed cathodic peak at ≈1.8 V in the CV curves in Figure 2d.

$$I_2 + 6H_2O \xrightarrow{\text{overcharge}} 2IO_3^- + 12H^+ + 10e^- \quad (2)$$

In addition, density functional theory (DFT) calculation indicates that the adsorption energy of I_2 on the N-doped carbon (0.3–0.7 eV) is substantially higher than the I_2 solvation energy in water (Figure 3c). Interestingly, the adsorption energy of IO_3^- on the N-doped carbon (1.3–3.1 eV) is much lower than the corresponding IO_3^- solvation energy in water (5.1 eV) (Figure 3d). This result reflects that IO_3^- is more easily dissolved into the aqueous electrolyte than I_2. The gradual dissolution of IO_3^- in electrolyte causes the loss of active cathode, thereby leading to the serious capacity decay of ZIABs.

Since electrolyte pH is a good indicator for the initial overcharge process of ZIABs, incorporating a suitable pH-responsive electrolyte into ZIABs is a feasible strategy to prevent the electrode degradation (I_2/IO_3^- and Zn/ZnO) and battery failure at overcharge state. We thus developed a series of pH-responsive electrolytes based on $ZnSO_4$ solution and various polymers with tertiary amine or pyridinic groups, such as poly[(2-dimethylamino)ethyl methacrylate] (PDMA), poly[(2-diisopropylamino) ethyl methacrylate] (PDPA) and poly(1-vinylpyrrolidone-co-2-dimethylaminoethyl methacrylate) (PVDM), poly(4-vinylpyridine) (P4VP), and poly(2-vinylpyridine) (P2VP). The resistances of electrolytes based on the above responsive polymers at different pH were measured by electrochemical impedance spectra (EIS).[44,45] Electrolyte pH was adjusted by adding dilute KOH solution. **Figures 4**a presents the resistances of electrolytes based on various responsive polymers along with the change of electrolyte pH (Figure S15, Supporting Information). As revealed, P2VP based electrolyte shows the largest resistance variations among different pH values, implying its remarkable sensitivity with respect to the pH change. In detail, P2VP based electrolyte at a pH of 4.0 has a low resistance of ≈10 Ω, which is almost the same as the pristine $ZnSO_4$ electrolyte (Figure S16, Supporting Information). When the pH of P2VP based electrolyte increases to 6.0, the resistance reaches up to 220 Ω (Figure 4a). This immense increase of resistance is ascribed to the deprotonation of quaternary pyridinic groups in P2VP, which is accompanied by the hydrophilic-to-hydrophobic sol–gel transition.[46] In the gel-state, the migration of Zn^{2+} is largely restrained. Importantly, the protonation of pyridinic groups in P2VP at the pH below 4.5 re-converts the polymer backbones from hydrophobic to hydrophilic nature. Thus, P2VP-based electrolyte recovers to a low resistance of 10 Ω after

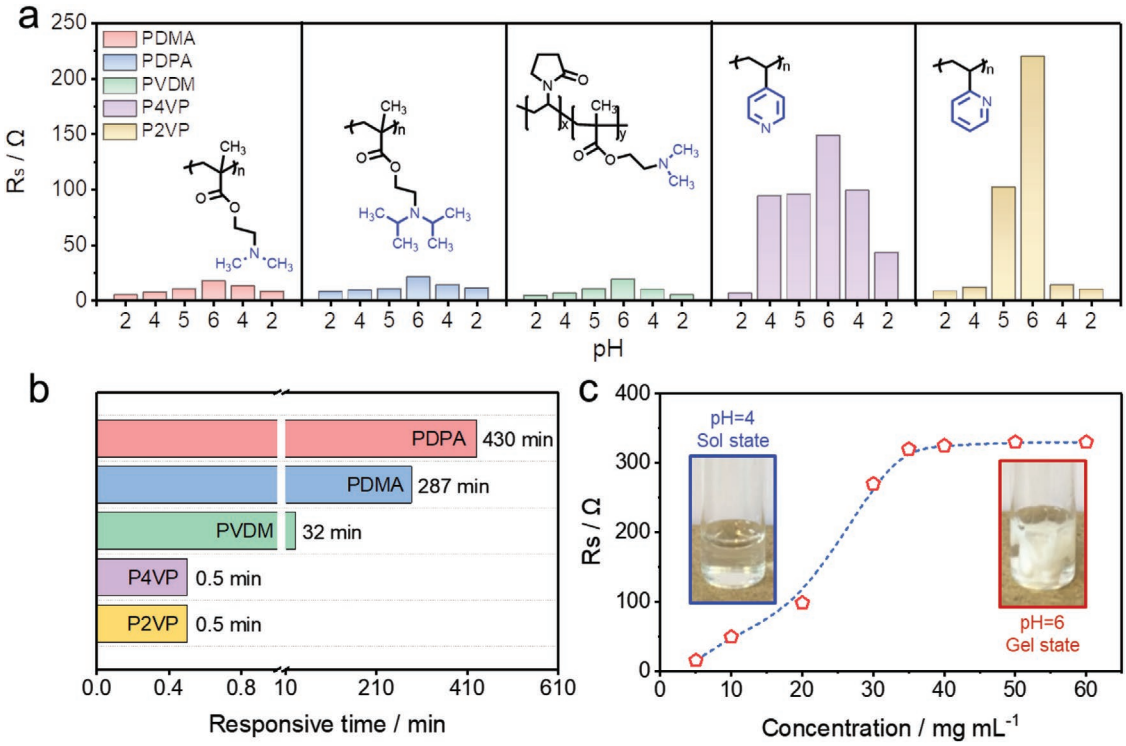

Figure 4. The pH-responsive properties of aqueous electrolytes based on various responsive polymers. a) The pH-dependent resistance values of the aqueous electrolytes based on PDMA, PDPA, PVDM, P4VP, and P2VP with the concentration of 30 mg mL^{-1}. b) The response times of the aqueous electrolytes based on PDMA, PDPA, PVDM, P4VP, and P2VP. c) The electrolyte resistances based on different concentrations of P2VP. Insets are the photographs showing the sol (pH = 4) and gel (pH = 6) states of the pH-responsive electrolyte with a P2VP concentration of 35 mg mL^{-1}.

the pH decreases to 4.0, indicating its highly reversible pH-responsive behavior.

Apart from the electrolyte resistances, the response time of the sol–gel transition is also crucial for the pH-responsive polymers. As shown in Figure 4b, P2VP and P4VP based electrolytes possess much faster response ability (less than 30 s) (Video S1, Supporting Information), in comparison with PVDM (≈30 min), PDMA and PDPA (>4 h). The short response time of P2VP and P4VP relies on the pyridinic groups with fast-kinetics of ionization/deionization.[46–48] Moreover, the potentiometric titration curve was collected for P2VP polymer in water. A plateau region was observed in the titration curve at around pH = 5.0 (Figure S17, Supporting Information) due to the presence of the ionizable pyridinic groups, suggesting that P2VP acts as a weak base in an acid–base equilibrium reaction. In addition, the sol-gel transition pH (inset in Figure 4c) was determined to be around 5.0 based on the UV–vis transmittance measurements (Figure S18, Supporting Information), which is consistent with the result from potentiometric titration curve. In addition, the concentration of P2VP in the $ZnSO_4$ electrolyte was optimized to be 35 mg mL^{-1} (Figure 4c). When the concentration of P2VP is above 35 mg mL^{-1}, the resistance of electrolyte at pH = 6.0 becomes stable along with the further increase of the P2VP concentration.

In order to demonstrate the smart over-charge self-protection ability of our developed pH-responsive electrolyte, SR-ZIABs were assembled by replacing traditional $ZnSO_4$ electrolyte with the pH-responsive P2VP based electrolyte. In the normal voltage window of 0.6–1.6 V, the fabricated SR-ZIABs exhibited a specific capacity of 142 mAh g^{-1} at 1.6 A g^{-1} (Figure S19, Supporting Information), which was nearly equivalent to ZIABs with the pure $ZnSO_4$ electrolyte (Figure S8, Supporting Information). As revealed in **Figure 5**a, once SR-ZIABs were overcharged to 1.95 V at a current density of 1.6 A g^{-1}, the subsequent discharge time exhibits a dramatic decrease, which indicates the pH-controlled switch-off behavior of SR-ZIABs at overcharge state. Even after the operation voltage windows recovered to the normal range (0.6–1.6 V), SR-ZIABs still exhibited very short discharge time (less than 20 s) with charge voltage steeply reaching the upper limit (1.6 V) and discharge voltage suddenly dropping to the lower limit (0.6 V). To mimic the practical charging condition, another charging mode by using constant voltage was used for SR-ZIABs (Figure 5b). After being overcharged at 1.95 V for 20 min, SR-ZIABs also showed short charge/discharge time (less than 20 s) in the subsequent cycle. Similarly, the overcharge switch-off behavior was confirmed by the CV curves (Figure S20a, Supporting Information). After charging to 1.95 V, the geometric areas of the CV curves of SR-ZIABs decreased by ≈94%. In addition, the self-protection ability of our SR-ZIABs under the overcharge voltage of 1.85 V was also demonstrated as shown in Figure S20b, Supporting Information.

EIS measurements were performed to investigate the resistance change of SR-ZIABs before (Figure 5c) and after (Figure 5d) overcharge. When SR-ZIABs were charged to 1.95 V, the charge transfer resistance of SR-ZIABs significantly increased by two

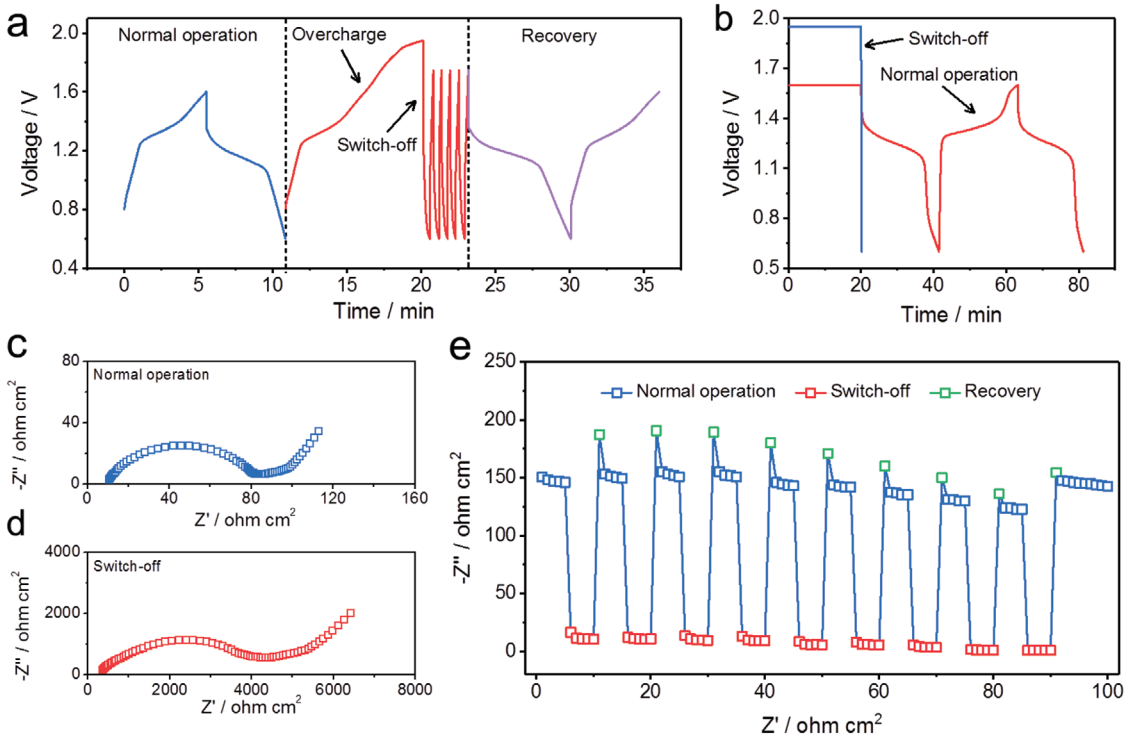

Figure 5. The reversible pH-responsive properties of the SR-ZIABs. a) The galvanostatic charge/discharge curves of SR-ZIABs in the voltage window of 0.6–1.6 V before and after the overcharge of SR-ZIABs to 1.95 V. b) The voltage-time curves of SR-ZIABs after constant-voltage charge at 1.6 and 1.95 V. The EIS plots of the SR-ZIABs c) before and d) after the overcharge process of SR-ZIABs. e) Cycling stability of the SR-ZIABs before and after overcharge of the SR-ZIABs to 1.95 V. The blue plots show the discharge capacities of the SR-ZIABs under normal operation. The red plots show the SR-ZIABs were switched off by overcharge. The green plots show the recovery of the SR-ZIABs by re-adjusting the electrolyte pH to the initial state.

orders of magnitude (from 85 to 4400 Ω cm^2). This is because that the adsorption of hydrophobic and non-conducting P2VP on the electrode surfaces (Figure S21, Supporting Information) blocks the Zn^{2+} diffusion at the electrolyte/electrode interface. Moreover, the electrolyte resistance increased from 9.7 to 360 Ω cm^2 when SR-ZIABs were charged to 1.95 V. Therefore, both solution resistance of the electrolyte and charge transfer resistance of the electrode greatly increased at overcharge state, thus inhibiting the electrode reactions of SR-ZIABs. When the electrolyte pH was re-adjusted to the initial value (4.0–4.5), P2VP deposited on electrode surface was re-dissolved and the electrolyte became ionically conductive again, so that the capacity of SR-ZIABs recovered to the initial value. Finally, the overcharge/recovery cycle stability measurements were performed for SR-ZIABs. The dilute sulfuric acid solution was used to re-adjust the electrolyte pH of the overcharged Zn–I_2 battery to the initial value. During the repeated overcharge/recovery processes, the specific discharge capacity of the SR-ZIABs decreased from 155 mAh g^{-1} under normal operation (0.6–1.6 V) to less than 10 mAh g^{-1} after the overcharge of SR-ZIABs to 1.95 V (Figure 5e). Clearly, the fabricated SR-ZIABs under overcharge conditions were rapidly switched off with capacity degradation to 6% of the initial capacity. When the pH was re-adjusted to the initial value, the specific capacity of SR-ZIABs was almost fully recovered. After ten overcharge/recovery cycles, the specific capacity of the SR-ZIABs still retained 146 mAh g^{-1} at 1.2 A g^{-1}, demonstrating the excellent reversibility of the overcharge/self-protection behavior.

In summary, we developed a novel kind of SR-ZIABs with smart self-protection function at the overcharge state. Our work demonstrated that charging ZIABs to above 1.6 V caused the rapid decrease of Coulombic efficiency and the increase of the electrolyte pH. The operando synchrotron X-ray diffraction together with UV–vis spectroscopy analysis revealed two serious side reactions of ZIABs at overcharge state, namely irreversible conversion from I_2 to $Zn(IO_3)_2$ at the cathode and from Zn to ZnO at the anode. These two side reactions caused the rapid capacity decay and battery failure of ZIABs under overcharge conditions. Using a pH-responsive electrolyte with reversible sol-gel transition and fast response time (less than 30 s), SR-ZIABs can be rapidly switched off with capacity degrading to 6% of the initial capacity under overcharge conditions, thereby preventing the irreversible side reactions (including H_2 generation and electrode degradation) and battery failure. This work opens the way to develop smart aqueous Zn batteries with self-protection ability at overcharge state.

Supporting Information

Supporting Information is available from the Wiley Online Library or from the author.

Acknowledgements

F.W., J.T., and Z.L. contributed equally to this work. This work was financially supported by the European Research Council (ERC) under the

European Union's Horizon 2020 research and innovation programme (grant agreement No 819698 and GrapheneCore2 785219), Deutsche Forschungsgemeinschaft (MX-OSMOPED project), and German Research Foundation (DFG) within the Cluster of Excellence. Y. Wu appreciates the financial support of NSFC (51425301 and U1601214). The authors acknowledge DESY (Hamburg, Germany), a member of the Helmholtz Association HGF, for the provision of synchrotron experimental facilities at P02.1. The authors also acknowledge the use of the facilities in Dresden Center for Nanoanalysis at Technische Universität Dresden, Center for Information Services and High-Performance Computing (ZIH) at Nanjing Tech University for computational resources.

Conflict of Interest

The authors declare no conflict of interest.

Keywords

battery overchange, battery self-protection, metal-I_2 batteries, stimulus-responsive batteries, Zn anodes

Received: January 13, 2020
Revised: February 8, 2020
Published online: March 5, 2020

[1] H. Sun, C. P. Kabb, Y. Dai, M. R. Hill, I. Ghiviriga, A. P. Bapat, B. S. Sumerlin, *Nat. Chem.* **2017**, *9*, 817.
[2] S. Mura, J. Nicolas, P. Couvreur, *Nat. Mater.* **2013**, *12*, 991.
[3] J. Lin, M. Lai, L. Dou, C. S. Kley, H. Chen, F. Peng, J. Sun, D. Lu, S. A. Hawks, C. Xie, F. Cui, A. P. Alivisatos, D. T. Limmer, P. Yang, *Nat. Mater.* **2018**, *17*, 261.
[4] A. H. Gelebart, D. J. Mulder, M. Varga, A. Konya, G. Vantomme, E. W. Meijer, R. L. B. Selinger, D. J. Broer, *Nature* **2017**, *546*, 632.
[5] H. Zhou, C. Xue, P. Weis, Y. Suzuki, S. Huang, K. Koynov, G. K. Auernhammer, R. Berger, H. J. Butt, S. Wu, *Nat. Chem.* **2017**, *9*, 145.
[6] H. Yang, W. R. Leow, T. Wang, J. Wang, J. Yu, K. He, D. Qi, C. Wan, X. Chen, *Adv. Mater.* **2017**, *29*, 1701627.
[7] A. Lee, M. Vörös, W. M. Dose1, J. Niklas, O. Poluektov, R. D. Schaller, H. Iddir, V. A. Maroni, E. Lee, B. Ingram, L. A. Curtiss, C. S. Johnson, *Nat. Commun.* **2019**, *10*, 4946.
[8] L. Li, S. Basu, Y. Wang, Z. Chen, P. Hundekar, B. Wang, J. Shi, Y. Shi, S. Narayanan, N. Koratkar, *Science* **2018**, *359*, 1513.
[9] F. Wang, H. Yang, J. Zhang, P. Zhang, G. Wang, X. Zhuang, G. Cuniberti, X. Feng, *Adv. Mater.* **2018**, *30*, 1800028.
[10] Z. Fang, Y. Zhang, X. Hu, X. Fu, L. Dai, D. Yu, *Angew. Chem., Int. Ed.* **2019**, *58*, 9248.
[11] C. Y. Wang, G. Zhang, S. Ge, T. Xu, Y. Ji, X. G. Yang, Y. Leng, *Nature* **2016**, *529*, 515.
[12] X. Wang, J. Gao, Z. Cheng, N. Chen, L. Qu, *Angew. Chem., Int. Ed.* **2016**, *55*, 14643.
[13] C. Wang, H. Wu, Z. Chen, M. T. McDowell, Y. Cui, Z. Bao, *Nat. Chem.* **2013**, *5*, 1042.
[14] Z. Chen, P. C. Hsu, J. Lopez, Y. Li, J. W. F. To, N. Liu, C. Wang, S. C. Andrews, J. Liu, Y. Cui, Z. Bao, *Nat. Energy* **2016**, *1*, 15009.
[15] Y. Sun, J. Lopez, H. W. Lee, N. Liu, G. Zheng, C. L. Wu, J. Sun, W. Liu, J. W. Chung, Z. Bao, Y. Cui, *Adv. Mater.* **2016**, *28*, 2455.
[16] J. Zhou, T. Qian, J. Liu, M. Wang, L. Zhang, C. Yan, *Nano Lett.* **2019**, *19*, 3066.
[17] A. Paolella, C. Faure, G. Bertoni, S. Marras, A. Guerfi, A. Darwiche, P. Hovington, B. Commarieu, Z. Wang, M. Prato, M. Colombo, S. Monaco, W. Zhu, Z. Feng, A. Vijh, C. George, G. P. Demopoulos, M. Armand, K. Zaghib, *Nat. Commun.* **2017**, *8*, 14643.
[18] J. Xu, Y. Chen, L. Dai, *Nat. Commun.* **2015**, *6*, 8103.
[19] Y. Zhao, Y. Zhang, H. Sun, X. Dong, J. Cao, L. Wang, Y. Xu, J. Ren, Y. Hwang, I. H. Son, X. Huang, Y. Wang, H. Peng, *Angew. Chem., Int. Ed.* **2016**, *55*, 14384.
[20] J. Zhao, K. K. Sonigara, J. Li, J. Zhang, B. Chen, J. Zhang, S. S. Soni, X. Zhou, G. Cui, L. Chen, *Angew. Chem., Int. Ed.* **2017**, *56*, 7871.
[21] Y. Huang, M. Zhong, Y. Huang, M. Zhu, Z. Pei, Z. Wang, Q. Xue, X. Xie, C. Zhi, *Nat. Commun.* **2015**, *6*, 10310.
[22] H. Sun, X. You, Y. Jiang, G. Guan, X. Fang, J. Deng, P. Chen, Y. Luo, H. Peng, *Angew. Chem., Int. Ed.* **2014**, *53*, 9526.
[23] H. Yang, Z. Liu, B. K. Chandran, J. Deng, J. Yu, D. Qi, W. Li, Y. Tang, C. Zhang, X. Chen, *Adv. Mater.* **2015**, *27*, 5593.
[24] M. Yu, X. Feng, *Joule* **2019**, *3*, 338.
[25] B. Li, Z. Nie, M. Vijayakumar, G. Li, J. Liu, V. Sprenkle, W. Wang, *Nat. Commun.* **2015**, *6*, 6303.
[26] Z. Wang, J. Huang, Z. Guo, X. Dong, Y. Liu, Y. Wang, Y. Xia, *Joule* **2019**, *3*, 1289.
[27] H. Pan, B. Li, D. Mei, Z. Nie, Y. Shao, G. Li, X. S. Li, K. S. Han, K. T. Mueller, V. Sprenkle, J. Liu, *ACS Energy Lett.* **2017**, *2*, 2674.
[28] J. Zhang, G. Jiang, P. Xu, A. G. Kashkooli, M. Mousavi, A. Yu, Z. Chen, *Energy Environ. Sci.* **2018**, *11*, 2010.
[29] H. Pan, Y. Shao, P. Yan, Y. Cheng, K. S. Han, Z. Nie, C. Wang, J. Yang, X. Li, P. Bhattacharya, K. T. Mueller, J. Liu, *Nat. Energy* **2016**, *1*, 16039.
[30] P. He, M. Yan, G. Zhang, R. Sun, L. Chen, Q. An, L. Mai, *Adv. Energy Mater.* **2017**, *7*, 1601920.
[31] K. Lu, Z. Hu, J. Ma, H. Ma, L. Dai, J. Zhang, *Nat. Commun.* **2017**, *8*, 527.
[32] P. Hu, T. Zhu, X. Wang, X. Wei, M. Yan, J. Li, W. Luo, W. Yang, W. Zhang, L. Zhou, Z. Zhou, L. Mai, *Nano Lett.* **2018**, *18*, 1758.
[33] C. Xia, J. Guo, P. Li, X. Zhang, H. N. Alshareef, *Angew. Chem., Int. Ed.* **2018**, *57*, 3943.
[34] D. Chao, W. Zhou, C. Ye, Q. Zhang, Y. Chen, L. Gu, K. Davey, S. Z. Qiao, *Angew. Chem., Int. Ed.* **2019**, *58*, 7823.
[35] H. Qiu, X. Du, J. Zhao, Y. Wang, J. Ju, Z. Chen, Z. Hu, D. Yan, X. Zhou, G. Cui, *Nat. Commun.* **2019**, *10*, 5374.
[36] W. Kaveevivitchai, A. Manthiram, *J. Mater. Chem. A* **2016**, *4*, 18737.
[37] D. Kralik, J. Jorne, *J. Electrochem. Soc.* **1980**, *127*, 2335.
[38] S. Biswas, A. Senju, R. Mohr, T. Hodson, N. Karthikeyan, K. W. Knehr, A. G. Hsieh, X. Yang, B. E. Koel, D. A. Steingart, *Energy Environ. Sci.* **2017**, *10*, 114.
[39] S. Thompson, F. L. Martucci, United States Patent, US6159631A, **2000**.
[40] Y. Li, L. Liu, H. Li, F. Cheng, J. Chen, *Chem. Commun.* **2018**, *54*, 6792.
[41] Y. K. Peng, L. Ye, J. Qu, L. Zhang, Y. Fu, I. F. Teixeira, I. J. McPherson, H. He, S. C. E. Tsang, *J. Am. Chem. Soc.* **2016**, *138*, 2225.
[42] V. Soundharrajan, B. Sambandam, S. Kim, M. H. Alfaruqi, D. Y. Putro, J. Jo, S. Kim, V. Mathew, Y. K. Sun, J. Kim, *Nano Lett.* **2018**, *18*, 2402.
[43] D. Kundu, S. H. Vajargah, L. Wan, B. Adams, D. Prendergast, L. F. Nazar, *Energy Environ. Sci.* **2018**, *11*, 881.
[44] Y. Zhu, F. Wang, L. Liu, S. Xiao, Z. Chang, Y. Wu, *Energy Environ. Sci.* **2013**, *6*, 618.
[45] X. Wang, F. Wang, L. Wang, M. Li, Y. Wang, B. Chen, Y. Zhu, L. Fu, L. Zha, L. Zhang, Y. Wu, W. Huang, *Adv. Mater.* **2016**, *28*, 4904.
[46] J. D. Willott, T. J. Murdoch, G. B. Webber, E. J. Wanless, *Prog. Polym. Sci.* **2017**, *64*, 52.
[47] G. Kocak, C. Tuncer, V. Bütün, *Polym. Chem.* **2017**, *8*, 144.
[48] J. Zhuang, M. R. Gordon, J. Ventura, L. Li, S. Thayumanavan, *Chem. Soc. Rev.* **2013**, *42*, 7421.